Fluid Dynamics & Materials Processing

Tech Science Press

DOI: 10.32604/fdmp.2022.018505

ARTICLE

Experimental Study on the Erosion of Pipelines under Different Load Conditions

Xuewen Cao[1], Ni Xiong[1], Jian Li[2], Zhenqiang Xie[1], Xuerui Zang[1] and Jiang Bian[1,*]

[1]Shandong Key Laboratory of Oil & Gas Storage and Transportation Safety, China University of Petroleum (East China), Qingdao, 266580, China

[2]Gulf Region Company of China Petroleum Engineering & Construction Co., Ltd., Beijing, 100120, China

[*]Corresponding Author: Jiang Bian. Email: bj@s.upc.edu.cn

Received: 29 July 2021 Accepted: 16 August 2021

ABSTRACT

The influence of the material stress state induced by internal and external forces on the erosion rate of pipelines has rarely been investigated in the literature. In order to fill this gap, using a tensile tester machine, a two–phase gas–solid particles jet erosion test was carried out considering a 316L stainless steel under different tensile stresses and different erosion angles. The results show that: 1) In the elastic range, with the increase of stress, the erosion rate manifests a rising trend; 2) In the metal plastic range, the increase of stress leads to a decrease of the erosion rate; 3) The erosion rate at a small erosion angle is more sensitive to the increment of stress. The present research demonstrates that the combined effect of erosion and material internal stress can contribute to determine the effective resistance of the vulnerable parts of piping systems (such as elbows or similar components).

KEYWORDS

Pipeline; load; solid particles; erosion

1 Introduction

In oil and gas gathering and transportation processes, sand particles are contained within the extracted oil and gas mixture. When particles move with the fluid to the elbow, tee, or valve, where the flow direction suddenly changes, their inertia will impact the inner pipe wall and possibly damage it. This process is known as erosion and causes serious safety hazards [1–3]. The main factors affecting the erosion rate are the particle velocity, the incident angle, particle properties, and target martial properties. Further, it was found that erosion could also be caused by working fluid hitting the pipe wall at high flow velocities [4]. Among the parameters, the particle velocity and the incident angle are closely related to the particle movement within the flow. On the other hand, both the particle and target martial properties are independent to flow. In current studies on erosion complications, the focus is mainly on the movement of particles within the pipeline, with little focus on the changes in target properties and their influences on the erosion process. However, in the actual pipeline operation, the pipeline is in a complex state of stress, which is not only generated by the internal pressure, but also by the external loads such as thermal expansion. Moreover, the elbow is a cause of stress concentration, in addition to being the most affected by erosion. Former studies revealed that stress affects the target material properties, in turn affecting the erosion rate. Therefore, studying the effect of stress on erosion is needed to better understand its implications.

By carrying fluids, the erosion wear can be divided into three categories: gas-solid erosion, liquid-solid erosion, and gas-liquid-solid three-phase erosion [5]. Among them, the gas-solid two-phase erosion experiment is widely used to study the erosion laws, mostly due to its relative simplicity and lower number of variables.

The primary factors affecting the erosion rate are particle speed, impact angle, and target properties [6–9]. The impact of particle velocity on the erosion rate is relatively intuitive; the greater the velocity, the greater the erosion rate, and vice versa. The impact angle affects the degree of erosion and wear. For the same experimental conditions, variations in impact angle will result in different erosion and wear mechanisms [10,11]. Finally, studies concerned with the influence of target properties on the erosion rate mostly focus on various types of target properties. For example, here are studies on the characteristic changes of material under various conditions.

Scattergood et al. [12,13] found that particles with different hardness greatly influence the erosion rate. Thus, problematic to estimate the effect of hardness using the indentation rupture theory. Andrzej et al. [14] experimentally studied how stress affects the surface coating erosion of hypoeutectoid steel. Further, Shellis et al. [15] studied the erosion caused by citric acid at low liquid velocities; the results have shown that repeated corrosion will affect the erosion. Introducing compressive stress into the steel reduced the surface roughness, thereby affecting the erosion morphology. Hence, stress concentration combined with corrosion in the elbow might reduce the pipeline erosion.

In currently used erosion models, the indentation hardness is commonly applied to determine the severity of cutting the material [16–22] and calculate the erosion rate. However, it cannot fully encompass how stress influences the material properties of the pipe, requiring further analysis.

The load pipeline bears can be roughly divided into four categories [23]:

1) Pressure loads caused by the internal temperature and pressure carried by fluid flowing through the pipeline;
2) Continuous external loads, which mainly include the pipe weight, the weight of its support and hanger accessories, outer pipe insulation material weight, and other uniformly distributed external loads;
3) Thermal loads generated by inconsistencies of temperatures during the installation and the operating states. The inconsistencies cause thermal expansion and contraction of the pipeline;
4) Occasional loads, which include occasional temporary loads such as fluid shocks and snow loads, which are generally not considered.

Finally, a comprehensive analysis has shown that stress has a significant impact on the properties of the pipe metal.

Studying the effects of stress on the target material properties started in 1932 by Kokubo et al. [24]. They carried out indentation experiments under various temperatures and pressures. The experimental results have revealed that the stress in metal materials significantly impacts the measured hardness. The tensile stress reduced the hardness of the sample materials by 5–12%. Frankel et al. [25] confirmed the conclusions of Kokubo and Kostron through additional experiments; tensile stress decreased the hardness value, while the compressive stress increased it slightly. Further, Sines et al. [26] studied the relationship between stress and hardness in high-carbon steel materials. A four-point bending experiment was used to induce stress on the target material, which was followed by measuring the indentation hardness. Further, the experimental conclusions have shown that tensile stress softened the material (<10%), while its compressive counterpart made it slightly harder (<1%). Additional analysis indicated that the tensile stress in a direction parallel to the sample surface increased the von Mises stress near the indentation crater. Thus, according to the plastic deformation theory, the increased von Mises stress increased the plastic deformation ability of the material. That resulted in a decrease in the sample hardness. On the

other hand, the compressive stress parallel to the sample surface reduced the von Mises stress near the indentation crater, increasing the sample hardness.

Based on the above-presented studies, it is evident that the stress state of the target material will significantly affect the hardness, in turn affecting the erosion behavior. Furthermore, in recent years, many studies on pipelines erosion behavior were carried out; however, only a few have considered the influence of pipeline loads on erosion. For this reason, a gas-solid two-phase jet erosion testing equipment was designed as a first step. Next, a tensile test machine was used to carry out an erosion experiment for different tensile stress conditions. Since the erosion mechanism change with the incident angle, erosion experiments under stress were carried out at incident angles of 30°, 45°, 60°, 75°, and 90°. The 316L metal was selected as the target material due to its wide application. Finally, the influence of stress on the erosion rate was investigated and the microscopic morphology of the erosion crater was analyzed to reduce the damage.

2 Experimental Process and Applied Materials

2.1 Gas-Solid Two-Phase Jet Erosion Experiment Equipment and Materials

Aiming to study the erosion process in target material under stress, a gas-solid two-phase jet erosion experiment was carried out for different tensile stress conditions. The schematic diagram of the experimental device is given in Fig. 1. The experimental system included a nitrogen gas source, an air nozzle, a tensile tester, and a specimen holder, among others.

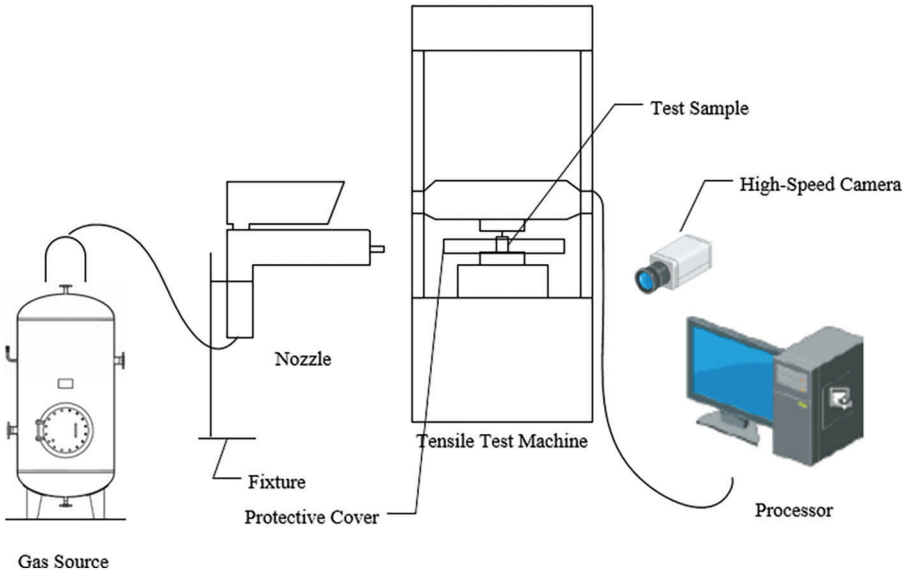

Figure 1: Schematic view of the experimental equipment

The tensile tester model used in the experiment was WANCE-ETM502B (technical parameters are provided in Table 1). The sample placement device, nozzle, and sample are shown in Fig. 2.

Table 1: The metal tensile tester machine parameters

Testing level	Testing range	Measuring range	Relative error	Testing machine resolution	Displacement resolution	Beam speed adjustment range
1	10 N to 2000 N	0.4% to 100% FS	± 1%	1/500000 FS	0.027 μm	0.001–500 mm/min

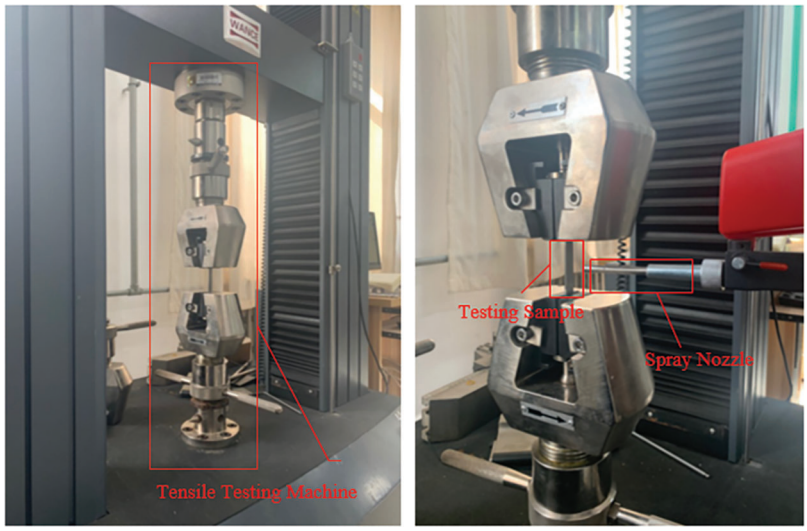

Figure 2: Tensile test machine, nozzle, and test sample

2.2 Materials

A nitrogen gas cylinder was used as the gas source in the experiment. The experimental test staple material was 316L stainless steel, chemical composition and mechanical properties of which are given in Table 2 and Table 3. In the experiment, the length, width, and height of the test sample were 72.4 mm × 11.5 mm × 2 mm, respectively. The erosive sand was made of Al_2O_3 particles, with the particle size was approximately 420 μm.

Table 2: Chemical composition of 316L stainless steel (mass fractions given in %)

Fe	C	Mn	Cr	Ni	Mo	Si	P
69.11	0.023	1.17	17.23	10.32	2.14	0.03	0.04

Table 3: Mechanical properties of the 316L stainless steel at 25°C

Tensile strength (MPa)	Conditional yield strength (MPa)	Yield strength (MPa)	Elastic modulus (GPa)	Poisson's ratio	Brinell hardness (HB)	Vickers hardness (HV)
≥480	≥177	270	206	0.299	≤187 HB	≤200

2.3 Experimental Procedure and Post-Processing

After assembling the experimental rig, the tensile tester machine is opened and the tensile force was adjusted to 0 N (which resulted in the stress of 0 MPa), 2300 N (100 MPa), 4600 N (200 MPa), 6900 N (300 MPa), 9200 N (400 MPa), and 11500 N (500 MPa), depending on the required testing conditions.

Samples were weighed before and after the erosion, experiment to obtain the masses M1 and M2, respectively. The total weight of erosion particles was recorded as Mp and was used to calculate the erosion rate. The experiments were replicated three times for each experimental condition and the average

of the three values was used as the final result to reduce error. The expression for calculating the total erosion rate is given as (1):

$$ER = \frac{M_1 - M_2}{M_p t} \tag{1}$$

where ER represents the sample mass loss caused by the unit mass of particles during the unit of time (the ER unit is kg/kg·h), M_1 is the mass of the test piece before the erosion (kg), M_2 is the mass of the test piece after the erosion (kg), M_p is the particle mass (kg), and t is the erosion time (h).

3 Experimental Results

3.1 Erosion Rate

The main factors affecting the erosion rate are the particle velocity, the incident angle, particle property, and target martial property, as mentioned earlier. In the experiment, the Al_2O_3 particles had the same size; therefore, the effects of particle properties were excluded. By keeping the outlet valve opening consistent, it was ensured that the particle velocity will be constant during the experiment. The incident angle was adjusted by fixing the nozzle. Therefore, the only experimental variable in the erosion experiment for a given incident angle was tensile stress.

The variation of total erosion rate with the stress and impact angle was obtained using the gas-solid two-phase experimental system (see Fig. 3). It can be seen that when stress increases from 0 MPa to 500 MPa, the total erosion rate fluctuated, meaning that the increase was not constant. The pattern was divided into two parts, the elastic range (0–200 MPa) in which the erosion rate rapidly increases with impact angles of 30°, 45°, 60°, 75°, and 90°, and the plastic range (300–500 MPa), where the erosion rate decreased slowly for all the impact angles.

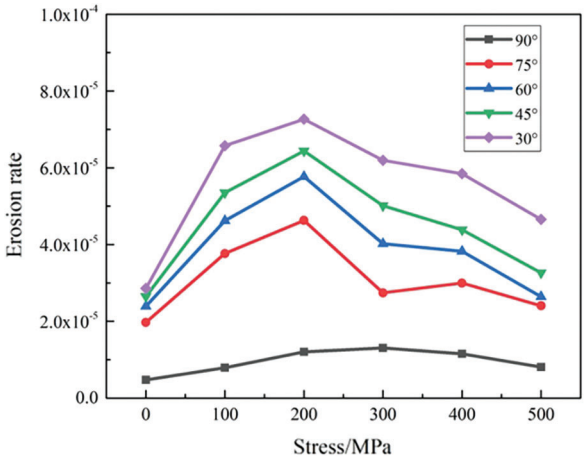

Figure 3: Stress-erosion rate diagram for various incident angles

Additionally, the erosion rate with a small incident angle was more sensitive to the stress increment. For the test sample with a 30° impact angle, the erosion rate at 0 MPa was 2.8591×10^{-5} kg/kg·h, while its value was 7.2666×10^{-5} kg/kg·h at 200 MPa. Hence, the erosion rate increased 2.5 times. In contrast, under the same stress condition with the impact angle of 90°, the erosion rate only increased 1.5 times.

Fig. 4 shows the macroscopic erosion morphology at 0 MPa, 200 MPa, and 500 MPa for incident angle 75°. The stress had a limited effect on the erosion pit aspect ratio; however, certain differences were observed at erosion pit edges at some stress conditions.

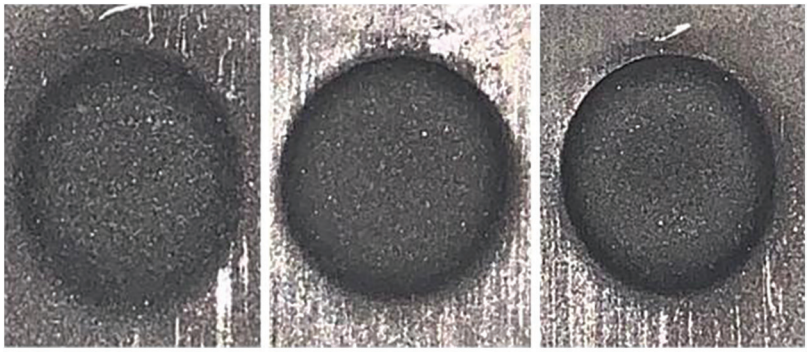

Figure 4: The macro morphology of 75° erosion pit; (a) 0 MPa, (b) 200 MPa, (c) 500 MPa

3.2 Micro-Morphology

Following the experiment, a wire was used to cut the test sample erosion position and the surface morphology of the erosion parts was scan using an electron microscope. The impact angle of the observed specimen was 90° and test piece stresses were 0 MPa, 100 MPa, 200 MPa, 300 MPa, 400 MPa, and 500 MPa, respectively. The surface image of the center pit part eroded under those conditions is shown in Fig. 5. The common feature of all micro-morphologies is that the erosion surface had a large number of pits and a rather small amount of scratches and flakes.

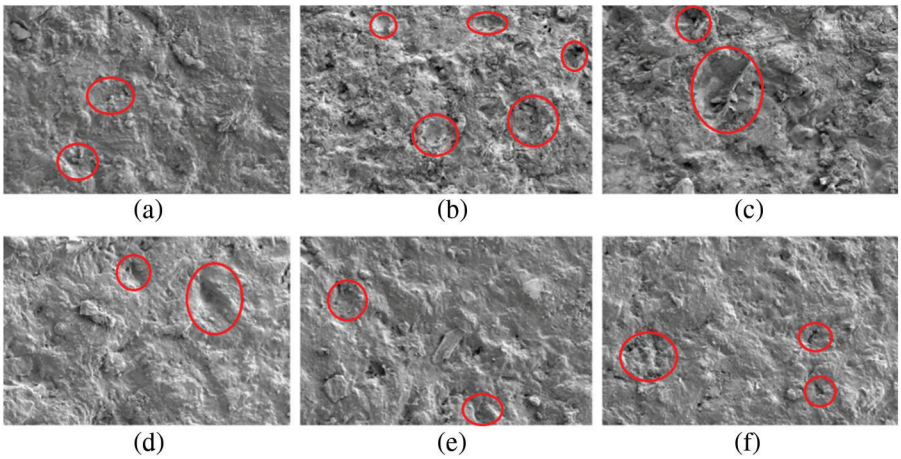

Figure 5: Scanning microscope image of the erosion crater; (a) 0 MPa, (b) 100 MPa, (c) 200 MPa, (d) 300 MPa, (e) 400 MPa, (f) 500 MPa

After observing the scanning electron microscope (SEM) pictures shown above, it can be seen that the erosion surface at 90° incident angle was dominated by pits caused by repeated particle impacts. Among them, the surface craters at the 0 MPa test sample were not noticeable and the overall surface morphology remained relatively flat. The density of surface craters started to increase with the 100 MPa test sample, which had a rugged surface with evident traces of repeated particle impacts. Further, the diameter of

surface craters became larger at 200 MPa, with the pit depth being much deeper compared to the 100 MPa test sample. Moreover, the surface pit diameters of the 300 MPa test sample were smaller than that of the 200 MPa sample; similarly, the pit depth was also lower. The surface of 400 MPa had no easily noticeable pits and was relatively flat. Similar was observed for the surface of the 500 MPa sample; there were practically no pits and the surface was flatter than that of the 400 MPa.

Based on the analysis above, it can be concluded that as the stress increases from 0 to 200 MPa, the surface impact marks gradually become noticeable, while the pit density and diameters increase. This implies that, within the elastic range, it is easier for particles to embed within the material and remove the surface pieces as the stress increases, causing increasing both the impact crater diameter and density. After particles impact the crater, a lip-like protrusion is formed around it. In the subsequent impact, the elevated material will be taken away, forming a crater through subsequent particles. This is consistent with the fact that those pits were found using the scanning electron microscope; however, there were no large lip-like protrusions around them. Additionally, in the plastic range, the material impact resistance increased with the increase in stress.

In addition to the pits, the forging signs such as small flakes and cracks can be seen on the target surface using the scanning electron microscope. According to the erosion theory proposed by Levy [27], the material surface will form both small flakes through particle impacts and a work-hardened plastic deformation layer prone to cracks under the action of external force. Under the repeated impacts and extrusion deformation, the work-hardened layer accelerated the shedding of small flakes from the surface. Small flakes and cracks were found on the test pieces at stresses of 0 MPa, 300 MPa, 400 MPa, and 500 MPa.

It should be noted that there were more flakes found on the 300 MPa and 400 MPa test samples, which also exhibited a greater flake size compared to the remaining samples. However, there are no visible flakes and cracks produced by forging on the surface of 100 MPa and 200 MPa samples. That is, the forging behavior had more influence on the surface morphology in the plastic stress zone. Thus, when the target is not stressed, inconspicuous pits and forging marks are found on the surface. When the target is in the elastic region, the density and diameter of surface pits increase with stress. On the other hand, when the target is in the plastic region, the surface morphology pits decrease as stress increases. The size of small flakes produced by the forging marks firstly increases with stress, then decreases after reaching the maximum value at 400 MPa. In other words, when the impact angle is 90°, the mechanism of removing the target surface material is closely related to its stress.

4 Conclusions

In this paper, a gas-solid two-phase erosion experiment was carried out at different stress; the relationship between the erosion rate, stress, and incident angle was obtained. Aiming to further study the erosion pattern, the influence of stress on the microscopic erosion morphology was analyzed using SEM. Based on the results, the following conclusions were made:

1) For the 316L metal in the elastic range 0–200 MPa, the erosion rate increases rapidly with the stress, weakening the material erosion resistance. In the plastic range (300 MPa to 500 MPa), the erosion rate decreased as the stress increased; however, pipelines used in engineering rarely reach the plastic stage. Thus, within the allowable engineering stress range, the stress will significantly increase the metal erosion rate.
2) Although within the elastic range, the erosion rate increased with the increase in stress for all incident angles. Moreover, the erosion rate at each angle increased at a different range. The erosion rate at large impact angles was not sensitive to stress as the erosion rate at 90° incident angle only increased 1.5 times, while at a small impact angle was it was more sensitive to the stress increment. The erosion rate at 30° incident angle increased 2.5 times.

3) The target material properties will change with the stress increment, leading to changes in both the diameter and depth of the pits, affecting the erosion rate. Lastly, by observing the microscopic morphology, it was also noticed that the stress will change the way the particles cut the material.
4) Erosion at elbows and similar places should consider the influence of stress. Thus, measures such as increasing the wall thickness, increasing the elbow curvature, and installing the additional features to reduce stress should be implemented to reduce the erosion risk and damage to the pipeline.

Funding Statement: This paper is financially supported from the National Natural Science Foundation of China (Grant No. 51874340), the Natural Science Foundation of Shandong Province (Grant No. ZR2018MEE004), and Project of China Petroleum Engineering Construction Co., Ltd., China (Grant No. CPECC2020KJ07).

Conflicts of Interest: The authors declare that they have no conflicts of interest to report regarding the present study.

References

1. Mccabe, L. P., Sargent, G. A., Conrad, H. (1985). Effect of micro structure on the erosion of steel by solid particles. *Wear, 105,* 257–277. DOI 10.1016/0043-1648(85)90072-9.
2. Islam, M. A., Farhat, Z. N., Ahmed, E. M., Alfantazi, A. M. (2013). Erosion enhanced corrosion and corrosion enhanced erosion of api x–70 pipeline steel. *Wear, 302(1–2),* 1592–1601. DOI 10.1016/j.wear.2013.01.041.
3. Macchini, R., Bradley, M. S. A., Deng, T. (2013). Influence of particle size, density, particle concentration on bend erosive wear in pneumatic conveyors. *Wear, 303(1–2),* 21–29. DOI 10.1016/j.wear.2013.02.014.
4. Hattori, S., Takinami, M. (2010). Comparison of cavitation erosion rate with liquid impingement erosion rate. *Wear, 269(3),* 310–316. DOI 10.1016/j.wear.2010.04.020.
5. Yao, J., Zhou, F., Zhao, Y. L. (2015). Investigation of erosion of stainless steel by two-phase jet impingement. *Applied Thermal Engineering, 88,* 353–362. DOI 10.1016/j.applthermaleng.2014.08.056.
6. MunOz–Escalona, P., Mridha, S., Baker, T. N. (2016). Effect of silicon carbide particle size on microstructure and properties of a coating layer on steel produced by TIG technique. *Advances in Materials and Processing Technologies, 2(4),* 1–10. DOI 10.1080/2374068X.2016.1246217.
7. Nan, L., Arabnejad, H., Shirazi, S. A., McLaury, B. S., Lan, H. (2018). Experimental study of particle size, shape and particle flow rate on erosion of stainless steel. *Powder Technology, 336,* 70–79. DOI 10.1016/j.powtec.2018.05.039.
8. Yang, Y., Cheng, Y. F. (2012). Parametric effects on the erosion-corrosion rate and mechanism of carbon steel pipes in oil sands slurry. *Wear, 276,* 141–148. DOI 10.1016/j.wear.2011.12.010.
9. Deng, T., Chaudhry, A. R., Patel, M., Hutchings, I., Bradley, M. (2005). Effect of particle concentration on erosion rate of mild steel bends in a pneumatic conveyor. *Wear, 258(1–4),* 480–487. DOI 10.1016/j.wear.2004.08.001.
10. Burstein, G. T., Sasaki, K. (2000). Effect of impact angle on the slurry erosion-corrosion of 304l stainless steel. *Wear, 240(1–2),* 80–94. DOI 10.1016/S0043-1648(00)00344-6.
11. Andrews, N., Giourntas, L., Galloway, A. M., Pearson, A. (2014). Effect of impact angle on the slurry erosion-corrosion of stellite 6 and SS316. *Wear, 320,* 143–151. DOI 10.1016/j.wear.2014.08.006.
12. Shipway, P. H., Hutchings, I. M., Scattergood, R. O. (1996). The role of particle properties in the erosion of brittle materials. *Wear, 193,* 105–113. DOI 10.1016/0043-1648(95)06694-2.
13. Srinivasan, S., Scattergood, R. O. (1988). Effect of erodent hardness on erosion brittle materials. *Wear, 128,* 139–152. DOI 10.1016/0043-1648(88)90180-9.
14. Andrzej, W., Hejwowski, T. (2008). Effect of stress on abrasive and erosive wear of steels and sprayed coatings. *Vacuum, 83(1),* 229–233. DOI 10.1016/j.vacuum.2008.04.004.
15. Shellis, R. P., Finke, M., Eisenburger, M., Parker, D. M., Addy, M. (2005). Relationship between enamel erosion and liquid flow rate. *European Journal of Oral Sciences, 113(3),* 232–238. DOI 10.1111/j.1600-0722.2005.00210.x.
16. Zhang, Y., Reuterfors, E. P., McLaury, B. S., Shirazi, S. A., Rybicki, E. F. (2007). Comparison of computed and measured particle velocities and erosion in water and air flows. *Wear, 263(1),* 330–338. DOI 10.1016/j.wear.2006.12.048.

17. Ahlert, K. R. (1994). *Effects of particle impingement angle and surface wetting on solid particle erosion of aisi 1018 steel.* The University of Tulsa, Tulsa, USA.
18. Mansouri, A. (2016). *A combined CFD–Experimental method for developing an erosion equation for both gas–sand and liquid–sand flows*. The University of Tulsa, Tulsa, USA.
19. Neilson, J. H., Gilchrist, A. (1968). Erosion by a stream of solid particles. *Wear, 11(2),* 111–122. DOI 10.1016/0043-1648(68)90591-7.
20. Oka, Y. I., Okamura, K., Yoshida, T. (2005). Practical estimation of erosion damage caused by solid particle impact: Part 1: Effects of impact parameters on a predictive equation. *Wear, 259(6),* 95–101. DOI 10.1016/j.wear.2005.01.039.
21. Oka, Y., Yoshida, T. (2005). Practical estimation of erosion damage caused by solid particle impact: Part 2: Mechanical properties of materials directly associated with erosion damage. *Wear, 259(6),* 102–109. DOI 10.1016/j.wear.2005.01.040.
22. Clark, R. A., Reissner, E. (1951). Bending of curved tubes. *Advances in Applied Mechanics, 2,* 93–122. DOI 10.1016/S0065-2156(08)70299-0.
23. Zhang, Y., Xu, X. (2021). Solid particle erosion rate predictions through lsboost. *Powder Technology, 388(9),* 517–525. DOI 10.1016/j.powtec.2021.04.072.
24. Kokubo, S. (1932). On the change in hardness of a plate caused by bending. *Science Reports of the Tohoku Imperial University (Series 1),* vol. 21, pp. 256–267.
25. Frankel, J., Scholz, W., Capsimalis, G., Korman, W. (1983). Residual stress measurement in circular steel cylinders. *International Ultrasonics Symposium, 7,* 1009–1012. DOI 10.1109/ULTSYM.1983.198215.
26. Sines, G., Carlson, R. (1952). Hardness measurement for determination of residual stresses. *ASTM Bulletin, 180,* 35–37.
27. Levy, A. V. (1986). The platelet mechanism of erosion of ductile metals. *Wear, 108(1),* 1–21. DOI 10.1016/0043-1648(86)90085-2.